Title: Hardness determination of bio-ceramics using laser-induced breakdown spectroscopy.

Authors:

J.S. Cowpe[1], R.D Moorehead[2], D. Moser[2], J.S. Astin[2], S. Karthikeyan[2], S.H. Kilcoyne[2], G. Crofts[3], R.D. Pilkington[2].

Affiliations:

[1]Isotope Geochemistry & Cosmochemistry Group, University of Manchester, Manchester, M13 9PL. UK

[2]Materials & Physics Research Centre, University of Salford, Salford, M5 4WT. UK

[3]School of Health, Sport & Rehabilitation Sciences, University of Salford, Salford, M5 4WT. UK

Corresponding author: J. S. Cowpe: john.cowpe@manchester.ac.uk
Isotope Geochemistry and Cosmochemistry Group, School of Earth, Atmospheric and Environmental Sciences, University of Manchester, Williamson Building 1.61, Oxford Road, Manchester, M13 9PL, UK. Telephone: +44-(0)161-275-3941

Abstract:

Laser-Induced Breakdown Spectroscopy (LIBS) was applied to the analysis of bio-ceramic samples. The relationship between sample hardness and LIBS plasma properties was investigated, with comparison to conventional Vickers hardness measurements. The plasma excitation temperature T_e was determined using the line-to-continuum ratio for the Si (I) 288.16 nm emission line; we have demonstrated a linear relationship between sample surface hardness and plasma temperature. Results indicate that hardness determination based on measurements of T_e offers greater reproducibility than Vickers hardness measurements, under the conditions considered here. The validity of spectroscopic diagnostics based on LTE was confirmed.

Keywords:

Glass ceramic, Hydroxyapatite, LIBS, Laser ablation, Plasma

1. Introduction

In recent years there has been a considerable focus on developing innovative implant materials that either integrate with the existing bone (non-resorbable bio-active materials), or act as temporary structures upon which the body heals itself and that are then subsequently dissolved (resorbable bio-active materials) [1]. Certain non-resorbable materials, such as crystalline apatite based ceramics, have been shown to be particularly bio-active as they exhibit a similar crystal structure to hydroxyapatite, the major mineral constituent of bone [2-4]. When developing these implant materials a rigorous characterization of their mechanical properties is required; the flexural strength, biaxial flexural strength and material hardness are major factors in determining the fracture resistance of the implant [5].

The hardness of a material is characterized by its resistance to permanent indentation and there are a number of different hardness tests that can be used [6]. One of the most commonly employed techniques is the Vickers hardness test that requires the optical measurement of the indented area related to an applied load; the hardness is measured using the Vickers hardness number (VHN). The Vickers hardness test can be time consuming, places geometric and size constraints on the samples that may be analysed and requires that samples have a good surface finish.

In this work we are assessing the potential of using Laser-Induced Breakdown Spectroscopy (LIBS) as a rapid, in-situ, virtually non-destructive method of determining material hardness for samples of all sizes and geometries; LIBS measurements are compared against Vickers hardness measurements of three apatite based glass ceramic samples of differing composition. It is envisaged that LIBS may

be used as an on-line diagnostic technique to regulate composition and hardness during large scale implant manufacture and may also be used to ascertain the hardness of bone prior to implant surgery.

LIBS is a powerful analytical tool capable of sampling solids, liquids and gases for research and industrial applications [7-14]. LIBS historically has been a qualitative technique but over recent years it has developed into a pseudo-quantitative materials micro-analysis technique, capable of determining elemental composition, providing suitable calibration has been performed beforehand [10]. Several excellent review articles [8-10, 12-16] regarding LIBS fundamentals, applications and experimental approaches have been published. LIBS is a very versatile analytical technique, and has been employed in numerous industrial [17-19], environmental [20-22] and archaeological [23-25] applications, to give but a few examples.

In the LIBS technique, high intensity pulsed laser radiation is focused onto the target sample, and if the laser power density exceeds a material specific threshold value, typically 10^{9} – 10^{14} Wm^{-2} [7], then the material is ablated as an expanding plume, propagating outwards from the target surface. The ablated material is composed of neutral particles, free electrons and ionic species, and may be considered as a high-temperature plasma, approximately 10^{3} - 10^{5} K [7-9]. Spectroscopic analysis of the optical emission from the excited plasma species can allow for characterization of the sample under investigation.

LIBS has previously been applied to surface hardness determination of calcified tissues [26,27]. It was found that the ratio of selected ionic to neutral Mg and Ca

emission lines followed a linear trend with surface hardness when comparing samples of human tooth enamel, shell and eggshell over a hardness range 100 – 350 VHN. The MgII/MgI ratio was found to be preferable over CaII/CaI as an indicator of surface hardness; the chosen Mg emission lines were deemed less susceptible to self absorption under the conditions of the study. The plasma shockwave velocity was found to be proportional to the surface hardness; it is believed that the speed of the shockwave mediates the ionization effectiveness, and thus the ratio of ionic to neutral species comprising the plasma [26,27]. We postulate herein that the plasma shockwave velocity may also therefore mediate the temperature of the laser-induced plasmas, and that plasma temperature determination techniques may be employed as an indicator of sample hardness, possibly reducing uncertainties resulting from emission line self absorption. We compare Vickers surface hardness measurements of three apatite based bio-ceramics against plasma excitation temperature as determined using the line to continuum ratio method.

2. Materials and Methods

2.1 Sample Synthesis

The three samples examined in this study were crystallized from a precursor glass in a method similar to those described previously [28-31]. The samples are designated as *A*, *B* and *C*, and were created from feedstock oxides, fluorides and carbonates; their percentage compositions by weight are listed in Table 1. For each sample the appropriate reagents were first weighed out in stoichiometric amounts (± 0.05g) and tumbled together for one hour to ensure a homogeneous distribution of the reagents. The mixed reagents were placed into a 99.9% pure alumina crucible and melted in the centre of a furnace that was pre-heated to 1440 °C. The molten glass was quenched

by pouring it into cold water; the resulting small pieces of glass were dried, ground, and sifted to separate the particulate sizes. Samples were cast by heating the glass particulates in an alumina crucible at 500˚C for 45 minutes, then at 1440˚C for a further 55 minutes; the preliminary warming stage was included to reduce the risk of thermal shock and thus avoid damage to the crucible. A cylindrical carbon mould of inner bore 14 mm was warmed to 575˚C thirty minutes prior to the end of the sample heat treatment. The molten glass was transferred to the carbon mould, and then returned to the furnace for a further hour at 575˚C. The glass rods were then allowed to cool to ambient temperature within the furnace over a period of 12 hours. Sample *A* was put through a two stage heat treatment; two isothermal stages were performed at 622˚C and 1040˚C, with hold durations of 2 hours and 3 hours respectively, with a ramp rate fixed at 10˚C/min. Samples *B* and *C* underwent a single stage heat treatment, with the isothermal hold taking place at 1060˚C for 1h with a ramp rate of 20˚C/min. A diamond wire saw was used to cut the 14mm diameter rods into 1.3mm (± 0.05mm) deep discs, which were subsequently polished on a Buehler Metaserv polishing wheel using P1200 (15.3 ± 1μm particulate size) for 20 minutes, until all cutting marks were removed.

2.2 Experimental Apparatus

The apparatus depicted in Figure 1 is designed for LIBS material analysis and plasma plume characterization and is described in greater detail elsewhere [32]. The system includes an Nd:YAG laser (Continuum, Surelite), frequency doubled to produce an output at 532 nm, with a 4-6 ns pulse length and the beam attenuated using neutral density filters to a pulse energy of 200 mJ incident on the target. Laser radiation was focused onto the target surface using a 150 mm plano-convex quartz lens, with a spot

diameter of approximately 400 μm at the target surface. The ablation target was mounted on an x-y translation stage; successive laser-induced plasmas were thus generated using a fresh area of the target surface. Targets were orientated perpendicular to the direction of laser beam propagation.

Optical emission from the plasma plumes was collected, at 90° to the direction of plume propagation, using a 2 meter long Roper Scientific optical fiber (transmission range: 190 – 1100 nm). The optical fiber was coupled to the entrance slit of an Acton Research Spectra Pro 500i 0.5 m imaging triple grating (150, 600, 2400 grooves per mm) spectrometer, with the spectrometer input slit width set to 10 microns. The output of the spectrometer was coupled to a Princeton Instruments PI-MAX ICCD camera that utilized a proximity focused MCP intensifier connected via a fiber-optic coupling to the CCD array; the 1024 × 256 pixel CCD array was thermoelectrically cooled to -20°C. All LIBS spectra were captured using the 2400 grooves per mm diffraction grating, with a corresponding linear dispersion of 0.02 nm per pixel. The laser power supply, camera and PC were synchronized using a Princeton Instruments ST-133A controller and programmable timing generator. The integration time for each acquisition was fixed at 500 ns throughout this study; the capture delay time was fixed at 4 μs after laser firing. The samples were degreased in solvent at room temperature before LIBS analysis to remove any surface contamination; 25 individual LIBS measurements were performed on each of the three samples under identical experimental conditions.

For the Vickers hardness measurements a Struers Duramin-2 hardness tester was used. The hardness tester features a diamond indenter in the shape of a square-based

pyramid with an apex angle of 136˚; this was forced into the sample under a load of 1 kg. The indentation diagonal of the resulting indent was measured using a calibrated optical microscope. 30 separate Vickers tests were performed for each of the three samples.

3. Results

3.1 SEM micrographs of sample surface and typical LIBS spectrum

Figure 2 presents two SEM micrographs of the sample surface; both images were captured using a Hitachi S-570 SEM at 10kV and 6000× magnification. Figure 2a shows the cleaved edge of a polished sample used for hardness testing, Figure 2b more clearly illustrates the surface texture of the sample, revealing the interlocking plate like nature of the crystallites.

Figure 3 shows a small wavelength range of a typical LIBS spectrum captured during analysis of bio-ceramic sample *B*. The spectrum was acquired with a delay time of 4 μs and an integration time of 500 ns, and is corrected for the spectral response of the detection system. The Mg (I) emission line at 285.21 nm displays considerable self reversal. The wavelengths of the emission lines identified in Figure 3 are tabulated in Table 2.

3.2 Plasma excitation temperature compared to VHN

It was postulated that the excitation temperature T_e could provide a reproducible diagnostic tool for determining surface hardness. The plasma excitation temperature was determined using the line-to-continuum ratio method [33,34] for the Si (I) 288.16 nm emission line; this particular line was chosen at it was clearly resolvable in every

LIBS spectrum captured for each sample. Self absorption of the Si (I) 288.16 nm emission line may be considered negligible under the conditions of this study as the transition is not associated with the ground state, and there is a relatively low concentration of silicon in each sample. Under LTE the excitation temperature may be considered to be equal to the electron temperature [35]. To employ the line-to-continuum ratio method, a Voigt curve was fitted to the 288.16 nm emission line in each data set; prior to analysis the spectra were corrected for the spectral response of the instrument, and the ICCD dark charge background subtracted. Using the parameters resulting from the Voigt fit to the 288.16 nm Si (I) emission line, and assuming LTE conditions prevail within the plasma, the plasma excitation temperature T_e may be calculated using Equation 1 [33,36].

$$\frac{\varepsilon_l}{\varepsilon_c}(\lambda) = C_r \frac{A_{21} g_2}{U_i} \frac{\lambda_c^2}{\lambda_l T_e} \frac{\exp\left(\frac{E_i - E_2 - \Delta E_i}{kT_e}\right)}{\left[\xi\left(1 - \exp\frac{-hc}{\lambda k T_e}\right) + G\left(\exp\frac{-hc}{\lambda k T_e}\right)\right]} \quad (1)$$

In Equation 1 the term C_r = 2.005 × 10^{-5} (s K), A_{21} is the transition probability, E_i is the ionization potential, E_2 is the upper state energy level, and g_2 the upper state statistical weight. ΔE_i represents the lowering of the ionization potential of atoms in the presence of a field of ions and is small enough to be deemed insignificant [33]. U_i is the partition function for a silicon ion, and was calculated in the range 5.66 – 5.68 over the temperature conditions of this study. G is the free-free Gaunt factor, which is assumed to be unity [33]. ξ is the Schluter-Bibermann free-bound continuum correction factor, and was calculated for Si vapor by Liu et al. as 1.4 [33]. ε_c represents the continuum emission coefficient and is derived from the baseline offset

of the Voigt fit; ε_c must be corrected for the measurement bandwidth $\Delta\lambda$ over which the spectral emission is integrated. ε_l is the integrated emission coefficient over the line spectral profile, and is given by the integrated area of the fitted Voigt curve. λ_c and λ_l are the continuum wavelength and line wavelength (nm) respectively; from the Voigt curve fit: $\lambda_c = \lambda_l = x_c$. The parameters used for plasma temperature determinations are summarized in Table 3 [33,37]. There is no simple analytical solution for Equation 1; as such an iterative program was employed to solve for T_e numerically. The Si^+ partition function is a dependent of temperature and therefore it was required to re-calculate U_i at each successive stage of the iterative solution for T_e. Values of T_e, and hence U_i, were found to converge to steady values after five cycles of this iterative process.

The plasma excitation temperature T_e versus Vickers hardness number (VHN) for the three samples is plotted in Figure 4. Each data point represents the average of 30 individual VHN tests and 25 individual LIBS acquisitions; the error bars indicate the standard deviations of these measurements. The straight line represents a linear fit to the data; it can be seen from Figure 4 that T_e does indeed follow a linear relationship with increasing surface hardness as expected. The percentage relative standard deviations (%RSD) for the Vickers hardness data were calculated to be in the range 3.9 - 4.9 %. The %RSD for the measurements of T_e yielded from the three samples was in the range 0.22 -0.25 %, and thus LIBS measurements of T_e may be considered to offer greater repeatability than conventional Vickers hardness measurements.

3.3 Plasma electron density and LTE considerations

The electron density of the laser ablation plasma N_e was determined from the Stark broadening of the 288.16 nm Si (I) emission line. The contributions of resonance and Doppler line broadening were deemed insignificant under the conditions of this study. Resonance broadening is negligible as the 288.16 nm Si (I) line is not associated with a ground state [33, 35]. The Doppler effect induces a broadening in line width for Si (I) 288.16 nm of less than 3.2×10^{-6} nm, assuming that the plasma temperature is the maximum determined in this study [38]. The electron density of the plasma relates to the Stark pressure broadening of the emission line profiles according to Equation 2 [39]:

$$\Delta\lambda_{1/2} = 2w\left(\frac{N_e}{10^{16}}\right) + 3.5A\left(\frac{N_e}{10^{16}}\right)^{1/4}\left(1 - 1.2N_D^{-1/3}\right)w\left(\frac{N_e}{10^{16}}\right) \quad (2)$$

where $\Delta\lambda_{1/2}$ is the FWHM broadening of the line, N_e is the plasma electron number density, here w represents the electron impact width parameter, A is the ion broadening parameter, and N_D is the number density of particles in the Debye sphere, given by Equation 3 [39]:

$$N_D = 1.72 \times 10^9 \frac{T^{3/2}}{N_e^{1/2}} \quad (3)$$

where T represents the plasma temperature. Due to the negligible ionic contribution to Stark broadening, Equation 3 may be simplified as shown in Equation 4 [39,40]:

$$\Delta\lambda_{1/2} = 2w\left(\frac{N_e}{10^{16}}\right) \quad (4)$$

The electron impact broadening width parameter *w* is temperature dependent, and was interpolated for each appropriate temperature from the values given by Griem [41]. The observed line profile is a convolution of the Stark broadening of the emission lines and the broadening contribution of the detection system. The instrument broadening contributes a Gaussian component to the observed line shape, the Stark effect a Lorentzian contribution to the observed line profile. A deconvolution of the Voigt fit to each spectrum was performed, with the Gaussian FWHM fixed as the instrumental broadening contribution; in this way the FWHM of the emission lines was determined. The instrumental broadening profile was found to be 0.04 nm, measured using several narrow emission lines from a cadmium hollow cathode lamp, and was determined under identical conditions to the LIBS measurements.

It is well known that typical LIBS plasmas generally do not exhibit LTE at very early stages of their expansion [42]; however, the measurements presented in this work were conducted at a delay time of 4 μs, which is considered sufficient for thermalization of the plasma to occur [35]. For any given plasma to be considered to be in LTE then the lower limit for the electron number density N_e must satisfy Equation 5 [35,39,43]:

$$N_e \ (\mathrm{cm}^{-3}) \geq 1.6 \times 10^{12}\, T^{1/2}\, \Delta E^{3} \quad (5)$$

where ΔE (eV) is the energy difference between the upper and lower states and T (K) is the plasma temperature. For the Si (I) 288.16 nm line transition, ΔE = 4.3 eV. Using the highest plasma temperature measured, T ~ 6500 K, yields a minimum electron density of $N_e \geq 1.03 \times 10^{16}$ per cm^3. From Equation 4, the electron densities of the plasmas considered in this study were calculated to be in the range 9.20×10^{16} – 1.3×10^{17} per cm^3. It can be seen that N_e was greater than the lower limit required for LTE throughout this study. It should also be noted that the criterion outlined in Equation 5 is a necessary, but not the only requirement for LTE [42].

4. General Conclusion

We have shown that the plasma excitation temperature T_e displays a linear dependence on sample hardness. Results indicate that hardness determination based on measurements of T_e offers greater reproducibility than those based on conventional Vickers hardness measurements under the conditions considered here. The validity of spectroscopic diagnostics based on LTE was confirmed. From the results of this preliminary study, it is envisaged that LIBS may be used as an on-line diagnostic technique to monitor composition and hardness during implant manufacture and may also be used to ascertain the hardness of bone prior to implant surgery.

Acknowledgments

The authors gratefully acknowledge support for this work from the Medical Research Council grant no. G0802650 ID90193.

References

[1] LL. Hench, Bioceramics: From Concept to Clinic. J. Am. Ceram. Soc. 74 (1991) 1487-1510.

[2] C.M. Gorman, R.G. Hill, Heat-pressed ionomer glass-ceramics. Part I: an investigation of low and microstructure. Dent. Mater. 19 (2003) 320-326.

[3] C.M. Gorman, R.G. Hill, Heat-pressed ionomer glass-ceramics. Part II. Mechanical property evaluation. Dent. Mater. 20 (2004) 252-261.

[4] Y. Liu, X. Sheng, X. Dan, Q. Xiang, Preparation of mica/apatite glass-ceramics biomaterials. Mater. Sci. Eng: C 26 (2006) 1390-1394.

[5] M.A. Lopes, F.J. Monteiro, J.D. Santos, Glass-reinforced hydroxyapatite composites: fracture toughness and hardness dependence on microstructural characteristics. Biomater. 20 (1999) 2085-2090.

[6] C.B. Ponton, D.R. Rawlings, Vickers indentation fracture toughness test: Part 1. Mater. Sci. Tech. 5 (1989) 865-872.

[7] D.A. Cremers, L.J. Radziemski, Handbook of laser-induced breakdown spectroscopy. John Wiley and Sons Ltd, 2006. p.23-97.

[8] S. Amoruso, R. Bruzzese, N. Spinelli, R. Velotta, Characterization of laser-ablation plasmas. J. Phys. B: At. Mol. Opt. Phys. 32 (1999) R131-R172.

[9] D.A. Rusak, B.C. Castle, B.W. Smith, J.D. Winefordner, Recent trends and the future of laser-induced plasma spectroscopy. Trends. Anal. Chem. 17 (1998) 453-461.

[10] J.M. Vadillo, J.J. Laserna, Laser-induced plasma spectrometry: truly a surface analytical tool. Spectrochim. Acta Part B 59 (2004) 147-161.

[11] F. Yueh, J.P. Singh, H. Zhang, Laser-Induced Breakdown Spectroscopy, Elemental Analysis. In: R.A. Meyers ed. Encyclopedia of Analytical Chemistry. John Wiley & Son Ltd, 2000. p. 2066-87.

[12] R.E. Russo, X.L. Mao, C. Liu, J. Gonzalez, Laser assisted plasma spectrochemistry: laser ablation. J. Anal. At. Spectrom. 19 (2004) 1084-1089.

[13] B. Sallé, P. Mauchien, S. Maurice, Laser-Induced Breakdown Spectroscopy in openpath configuration for the analysis of distant objects. Spectrochim. Acta Part B 62 (2007) 739-768.

[14] E. Tognoni, V. Palleschi, M. Corsi, G. Cristoforetti, Quantitative micro-analysis by laser-induced breakdown spectroscopy: a review of the experimental approaches. Spectrochim. Acta Part B 57 (2002) 1115-1130.

[15] L.J. Radziemski, From LASER to LIBS, the path of technology development. Spectrochim. Acta Part B 57 (2002) 1109-1113.

[16] R. Noll, H. Bette, A. Brysch, M. Kraushaar, I. Mönch, L. Peter, V. Sturm, Laser induced breakdown spectrometry - applications for production control and quality assurance in the steel industry. Spectrochim. Acta Part B 56 (2001) 637-649.

[17] R. Noll, I. Mönch, O. Klein, A. Lamott, Concept and operating performance of inspection machines for industrial use based on laser-induced breakdown spectroscopy. Spectrochim. Acta Part B 60 (2005) 1070-1075.

[18] L. Barrette, S. Turmel, On-line iron-ore slurry monitoring for real-time process control of pellet making processes using laser-induced breakdown spectroscopy: graphitic vs. total carbon detection. Spectrochim. Acta Part B 56 (2001) 715-723.

[19] L. St-Onge, E. Kwong, M. Sabsabi, E.B. Vadas, Rapid analysis of liquid formulations containing sodium chloride using laser-induced breakdown spectroscopy. J. Pharmaceut. Biomed. 36 (2004) 277-284.

[20] R.S. Harmon, F.C. De Lucia, A.W. Miziolek, K.L. McNesby, R.A. Walters, P.D. French, Laser-induced breakdown spectroscopy (LIBS) – an emerging field-portable sensor technology for real-time, in-situ geochemical and environmental analysis. Appl. Geochem. 21 (2006) 730-747.

[21] N.K. Rai, A.K. Rai, LIBS -An Efficient Approach for the Determination of Cr in industrial wastewater. J. Hazard. Mater. 150 (2008) 835-838.

[22] M.A. Gondal, T. Hussain, Determination of poisonous metals in wastewater collected from paint manufacturing plant using laser-induced breakdown spectroscopy. Talanta 71 (2007) 73-80.

[23] A. Kaminska, M. Sawczak, K. Komar, G. Sliwinski, Application of the laser ablation for conservation of historical paper documents. Appl. Surf. Sci. 253 (2007) 7860-7864.

[24] A. Brysbaert, K. Melessanaki, D. Anglos, Pigment analysis in Bronze Age Aegean and Eastern Mediterranean painted plaster by laser-induced breakdown spectroscopy (LIBS). J. Arch. Sci. 33 (2006) 1095-1104.

[25] F.J. Fortes, M. Cortés, M.D. Simón, L.M. Cabalín, J.J. Laserna, Chronocultural sorting of archaeological bronze objects using laser-induced breakdown spectrometry. Anal. Chim. Acta 554 (2005) 136-143.

[26] Z.A. Abdel-Salam, Z. Nanjing, D. Anglos, M.A. Harith, Effect of experimental conditions on surface hardness measurements of calcified tissues via LIBS. Appl. Phys. B 94 (2009) 141-147.

[27] Z.A. Abdel-Salam, A.H. Galmed, E. Tognoni, M.A. Harith, Estimation of calcified tissues hardness via calcium and magnesium ionic to atomic line

intensity ratio in laser induced breakdown spectra. Spectrochim. Acta Part B 62 (2007) 1343-1347.

[28] P.M. Bentley, S.H. Kilcoyne, N.L. Bubb, C. Ritter, C. Dewhurst, D.J. Wood, Kinetic neutron diffraction and SANS studies of phase formation in bioactive machinable glass ceramics. Biomed. Mater. 2 (2007) 151-157.

[29] D. Wood, R. Hill, Structure-property relationships in ionomer glasses. Clin. Mater. 7 (1991) 301-312.

[30] D.J. Wood, R. Hill, Glass ceramic approach to controlling the properties of a glass-ionomer bone cement. Biomater. 12 (1991) 164-170.

[31] A. Clifford, R. Hill, Apatite-mullite glass-ceramics. J. Non-cryst. solids, 196 (1996) 346-351.

[32] J.S. Cowpe, J.S. Astin, R.D. Pilkington, A.E. Hill, Application of Response Surface Methodology to laser-induced breakdown spectroscopy: Influences of hardware configuration. Spectrochim. Acta Part B 62 (2007) 1335-1342.

[33] H.C. Liu, X.L. Mao, J.H. Yoo, R.E. Russo, Early phase laser induced plasma diagnostics and mass removal during single-pulse laser ablation of silicon. Spectrochim. Acta Part B 54 (1999) 1607-1624.

[34] H.R. Griem, Principles of Plasma Spectroscopy. Cambridge University Press, 1997. p.187-212.

[35] A.P. Thorne, Spectrophysics. Chapman and Hall Science Paperbacks, 1974. p. 354-357.

[36] G.J. Bastiaans, R.A. Mangold, The calculation of electron density and temperature in Ar spectroscopic plasmas from continuum and line spectra. Spectrochim. Acta Part B 40 B (1985) 885-892.

[37] D.R. Lide, editor. CRC Handbook of Chemistry and Physics, CRC Press, 1988.

[38] J.S. Cowpe, J.S. Astin, R.D. Pilkington, A.E. Hill, Temporally resolved laser induced plasma diagnostics of single crystal silicon - Effects of ambient pressure. Spectrochim. Acta Part B 63 (2008) 1066-1071.

[39] M. Milán, J.J. Laserna. Diagnostics of silicon plasmas produced by visible nanosecond laser ablation. Spectrochim. Acta Part B 56 (2001) 275-288.

[40] N.M. Shaikh, B. Rashid, S. Hafeez, Y. Jamil, M.A. Baig, Measurement of electron density and temperature of a laser-induced zinc plasma. J. Phys. D 39 (2006) 1384-1391.

[41] H.R. Griem, Plasma Spectroscopy. McGraw-Hill Inc., 1964.

[42] G. Cristoforetti, A. De Giacomo, M. Dell'Aglio, S. Lagnaioli, E. Tognoni, V. Palleschi, N. Omenetto, Local Thermodynamic Equilibrium in Laser-Induced Breakdown Spectroscopy: Beyond the McWhirter criterion. Spectrochim. Acta Part B 65 (2010) 86-95.

[43] R.W.P. McWhirter, in Plasma Diagnostic Techniques, R.H. Huddlestone and S.L Leonard Eds. (Academic Press, New York, 1965), Chap.5, pp. 201-264.

Table(s)

Table 1: Percentage composition of samples

Sample	% composition by weight							
	MgO	SiO_2	Al_2O_3	MgF_2	$BaCO_3$	CaF_2	$CaCO_3$	P_2O_5
A	12.00	27.45	8.37	8.96	14.33	1.59	18.66	8.65
B	14.77	35.55	12.55	10.11	16.17	0.60	7.01	3.25
C	13.30	31.25	10.33	9.50	15.19	1.12	13.18	6.11

Table 2: Emission line identification for LIBS spectrum presented in Figure 3

Wavelength (nm)	Species
277.67	Mg (I)
277.83	Mg (I)
277.98	Mg (I)
278.14	Mg (I)
278.30	Mg (I)

Wavelength (nm)	Species
279.55	Mg (II)
280.27	Mg (II)
285.21	Mg (I)
288.16	Si (I)

Table 3: Parameters used for plasma excitation temperature determination

Transition (nm)	A_{21} ($10^8 s^{-1}$)	g_2	E_2 (eV)	E_i (eV)	U_i	ξ	G	C_r (sK)
Si (I) 288.16	1.89	3	5.028	8.151	5.66 →5.68	1.4	1	2.005×10^{-5}

List of figure captions

Figure 1: The LIBS apparatus.

Figure 2: SEM micrographs of the bio-ceramic sample surface, 6000× magnification.

Figure 3: Typical LIBS spectrum captured during analysis of bio-ceramic sample *B*. Emission lines corresponding to neutral magnesium species (Mg I), ionic magnesium species (Mg II) and neutral silicon atoms (Si I) are identified. The spectrum was acquired with a delay time of 4 μs and an integration time of 500 ns, and is corrected for the spectral response of the detection system.

Figure 4: Plasma excitation temperature versus Vickers number (VHN). Each data point represents the average of 30 VHN tests versus the average of 25 individual LIBS spectra, error bars represent the standard deviation of these measurements.

Figure(s)

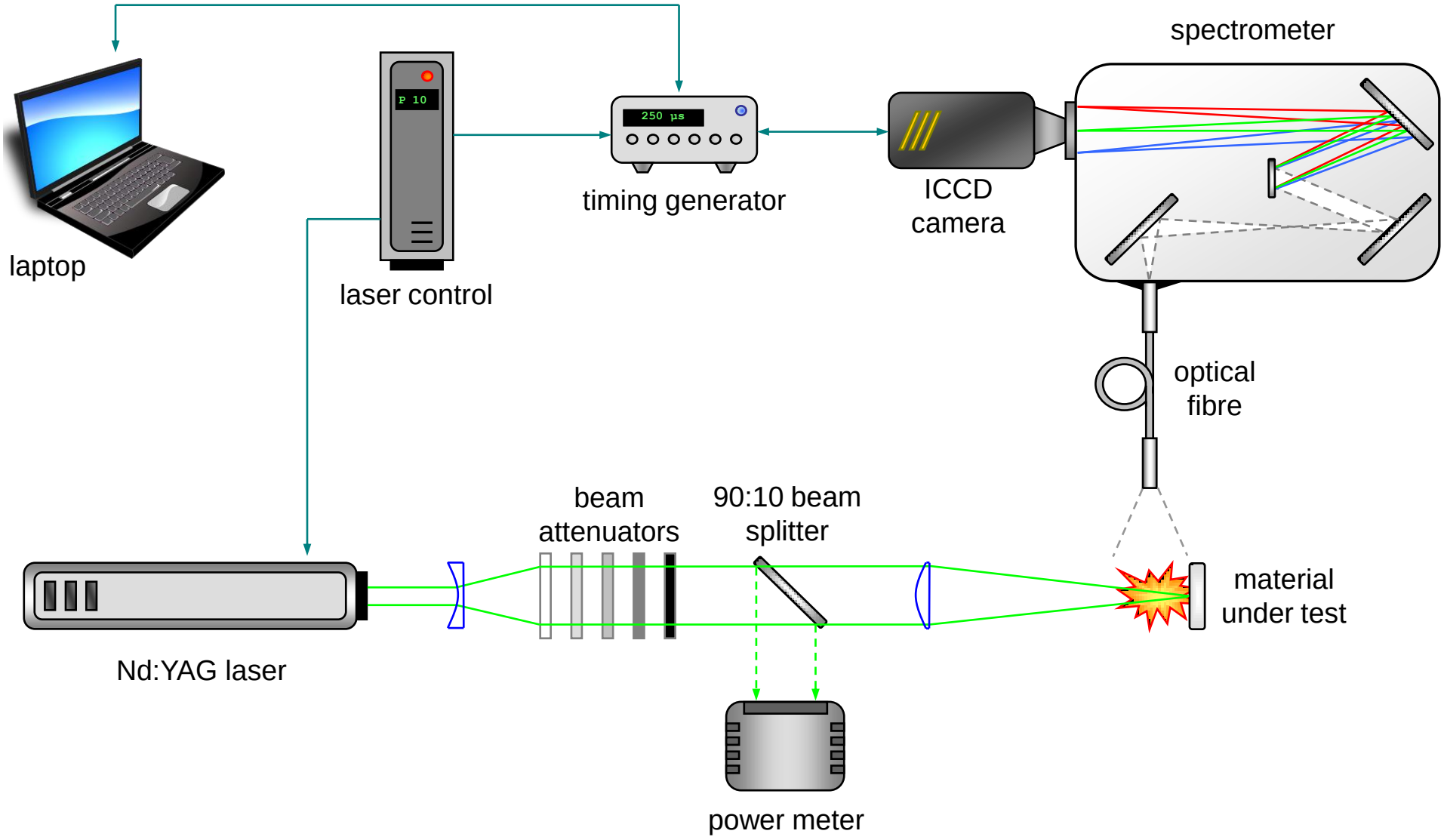
laptop
P 10
laser control
250 µs
timing generator
ICCD
camera
spectrometer
optical
fibre
beam
attenuators
90:10 beam
splitter
material
under test
Nd:YAG laser
power meter

Figure(s)

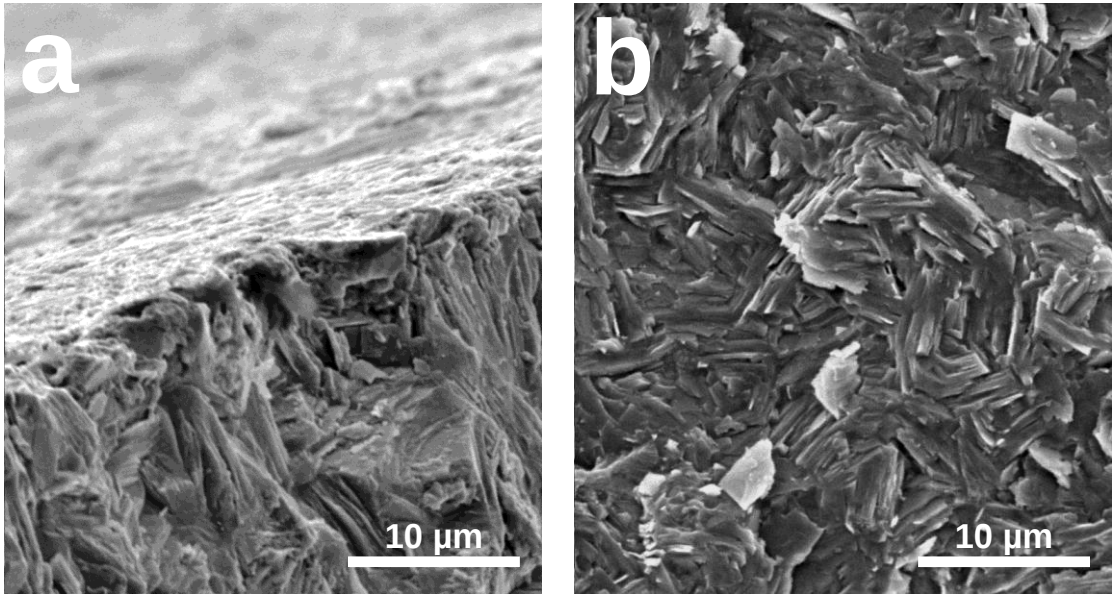

Figure(s)

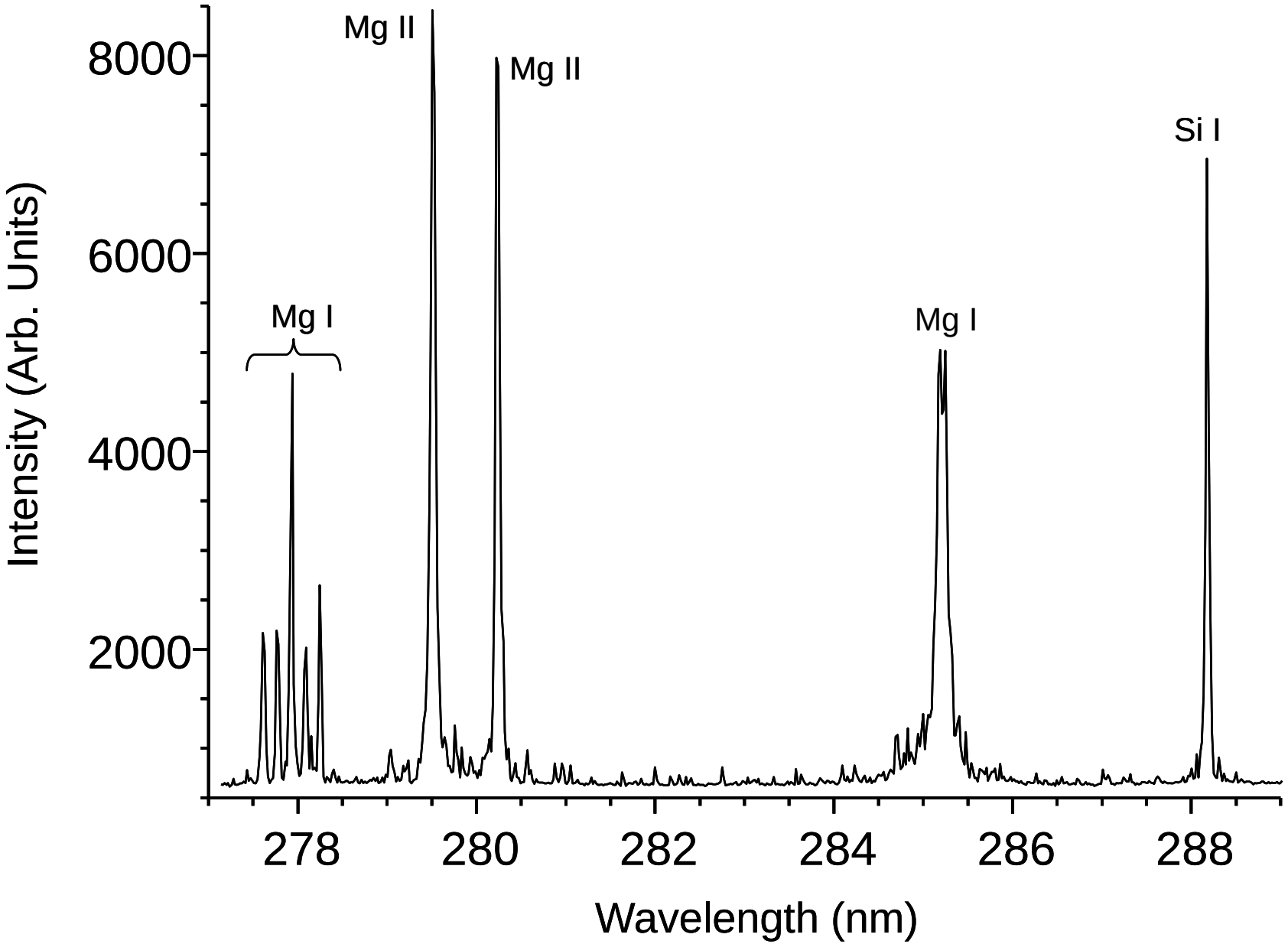
Mg II
Mg II
Si I
Mg I
Mg I
8000
6000
4000
2000
Intensity (Arb. Units)
278
280
282
284
286
288
Wavelength (nm)

Figure(s)

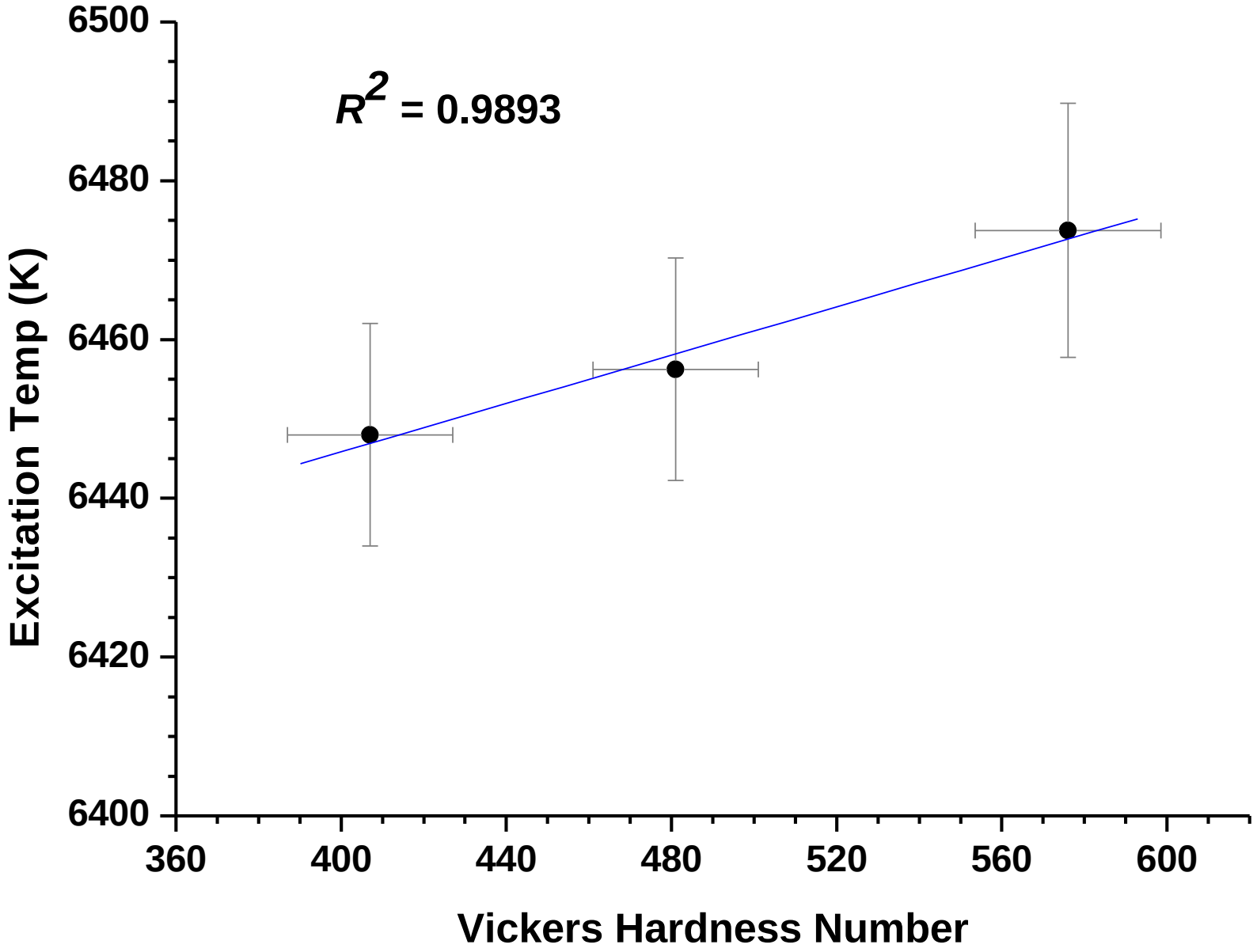
R^2 = 0.9893
Excitation Temp (K)
6500
6480
6460
6440
6420
6400
360
400
440
480
520
560
600
Vickers Hardness Number